Inelastic neutron scattering at the magnetic Brillouin zone boundary in antiferromagnetic Mn(13.7% Ni) alloy

2000 J. Phys.: Condens. Matter 12 161

(http://iopscience.iop.org/0953-8984/12/2/306)

J. Phys.: Condens. Matter **12** (2000) 161–176. Printed in the UK PII: S0953-8984(00)00475-6

Inelastic neutron scattering at the magnetic Brillouin zone boundary in antiferromagnetic Mn(13.7% Ni) alloy

J Jankowska-Kisielińska†, K Mikke†, B Hennion‡ and J J Milczarek†

† Institute of Atomic Energy, 05-400 Otwock, Świerk, Poland

‡ Laboratoire Léon Brillouin, CE-Saclay, 91191 Gif sur Yvette Cédex, France

Received 31 December 1998, in final form 14 July 1999

Abstract. This is the first systematic study of the spin excitations around the MBZ boundary points in γ-Mn alloy. The magnetic inelastic neutron scattering was measured in the antiferromagnetic Mn(13.7% Ni) alloy in a sample with unequal domain distribution in the temperature range 0.025 T_N–1.15 T_N. The evidence of the magnetic excitations around the MBZ boundary points equivalent to the MBZ centres in γ-Mn alloy is presented. At low temperatures these excitations differ from excitations observed around the MBZ centres; they are rather similar to excitations observed above T_N. When the temperature increases up to T_N the excitations observed around MBZ centres become more similar to those around the MBZ boundary equivalent points. The results of the analysis are consistent with the general features of spin fluctuations.

1. Introduction

The spin wave dispersion relation for many magnetic systems is measurable by inelastic neutron scattering (INS) in the whole Brillouin zone. In the case of 3d magnetic metals and alloys it is extremely difficult to detect spin waves up to the zone boundary because dispersion relations are very steep and at high energy one comes into the area of Stoner excitations. Low energy spin excitations at the magnetic zone boundary have not been observed in 3d metals and alloys except γ-manganese alloys (Vintaykin *et al* 1981, Mikke *et al* 1983).

Against the background of recent advances in understanding the spin dynamics close to and above the Curie temperature in Fe, Ni and other 3d ferromagnets our work provides an essential extension. The analysis of these excitations in 3d ferromagnets in terms of formulae for critical spin fluctuations resulted in a surprisingly consistent picture in wide range of energy and temperature (for reviews see Moriya 1985, Böni *et al* 1993). The 3d antiferromagnets are more complex and require much more refined tools both in experiment and theory. They offer however the possibility to test the extention of the formulae for critical scattering not only to the paramagnetic but also to the antiferromagnetic phase. This possibility appears in particular in the incommensurate SDW structure in chromium and in the single-Q AF1 structure of the γ-manganese alloys.

The aim of the reported experiment was to investigate the magnetic excitations in the γ-Mn(13.7% Ni) alloy around the specific points at the magnetic Brillouin zone (MBZ) boundary. In a polydomain sample these points coincide with the MBZ centres for domains with different orientation. The presence of the low energy inelastic neutron scattering around those points was observed by us earlier in a single domain sample of the γ-Mn–Cu alloy (Mikke *et al* 1983). We observed similar effects in the polydomain sample of Mn(13.7% Ni)

0953-8984/00/020161+16$30.00

alloy with unequal domain distribution, when we studied the spin waves around the MBZ centre (Jankowska-Kisielińska *et al* 1997a). The nature of these excitations was not identified. The critical scattering at 'silent satellites' observed recently in chromium (Sternlieb *et al* 1995) seems to have the same origin. The present experiment is a systematic study of the temperature dependence of these excitations.

A brief information on the results of the present experiment was given at the *ISNS '97 Conference* (Mikke *et al* 1998). Here we present the results of the full data analysis. In section 2 we present the consideration of the possibility of the extension of the critical spin fluctuation features to the paramagnetic and antiferromagnetic phase. We consider the surroundings of the real MBZ centre and of the point at the MBZ boundary equivalent to the MBZ centre for magnetic domains with different domain orientation. Section 3 contains: the investigated sample characteristics, the range of measurements, the experimental details and some examples of the measured distributions. Data analysis presented in section 4 is performed in terms of paramagnetic scattering in the paramagnetic region. Below T_N the analysis is done in terms of the scattering on damped spin waves around the MBZ centre and in terms of the Lorentzian-shape diffuse scattering around the 'unfulfilled' MBZ centre.

2. Preliminaries

The condition for magnetism to appear, in terms of the generalized magnetic susceptibility tensor $\chi(Q,\omega)$, is its singularity for $\omega = 0$, at some temperature $T_{cr} > 0$, and some wavevector $Q = Q_0$. In γ-manganese alloys which form AF1 structure below T_N, the singularity of magnetic susceptibility is expected for three Q_0 vectors: $Q_{01} = 2\pi/c[001]$, $Q_{02} = 2\pi/a[100]$, $Q_{03} = 2\pi/a[010]$ (and other translationally equivalent $Q_0 + G$, where G is the atomic reciprocal lattice vector). In alloys with high manganese content the AF1 structure is single Q, so only one of the above three Q_0 vectors is chosen to form the magnetic reciprocal lattice in a given domain. The corresponding reciprocal lattice points become the MBZ centres. The reciprocal lattice points corresponding to two other types of vector we call the 'unfulfilled' MBZ centres.

The neutron magnetic scattering cross-section is given by the formula of Van Hove (1954):

$$\frac{\mathrm{d}^2\sigma}{\mathrm{d}\Omega\,\mathrm{d}\omega} \propto \frac{k_f}{k_0}\sum_{\alpha\beta}\left(\delta_{\alpha\beta} - \frac{Q_\alpha Q_\beta}{|Q|^2}\right)\frac{2\overline{h}}{1-\exp(-\overline{h}\omega/k_BT)}\mathrm{Im}\chi^S_{\alpha\beta}(Q,\omega) \qquad (1)$$

where k_0 and k_f are the incident and scattered neutron wavevectors, $Q = |k_f - k_0|$ and the other symbols have the common meaning.

In the isotropic antiferromagnetic system with continuous transition, above T_N, for $|Q - Q_0 - G| \ll Q_0$, and $\omega < \omega_c$ (where ω_c is the cut-off frequency), the magnetic susceptibility $\chi(Q,\omega)$ can be approximated by the expansion to the lowest order in $|q| = |Q - Q_0 - G|$ and ω (as shown in different models by e.g. Halperin and Hohenberg 1969, Izuyama *et al* 1963, Moriya 1985):

$$\chi^{-1}(Q,\omega) = \chi^{-1}(Q_0,0) + aq^2 - \mathrm{i}c\omega \qquad (2)$$

where the coefficients a and c are expressed in terms of the model parameters. In the Stoner model of an itinerant system they depend on the band structure and the intraatomic exchange integral, and weakly depend on temperature. $\chi(Q_0,0)$ is the static staggered susceptibility and it diverges at T_N.

Above T_N the neutron scattering cross-section, being proportional to $\mathrm{Im}(Q,\omega)$, has in this approximation the known form:

$$\frac{\mathrm{d}^2\sigma}{\mathrm{d}\Omega\,\mathrm{d}\omega} \propto \frac{\omega}{1-\exp(-\overline{h}\omega/kT)}\chi(Q_0,0)\frac{\Gamma_0}{\omega^2+\Gamma^2(q)} \qquad (3)$$

where $\Gamma(q) = \Gamma_0 + Aq^2$, $\Gamma_0 = c^{-1}\chi^{-1}(Q_0, 0)$, $A = ac^{-1}$.

In fact, in the fcc lattice with antiferromagnetic interaction leading to the AF1 structure we should distinguish two components of magnetic susceptibility tensor parallel and perpendicular to the Q_0 vector. They should be different for fcc manganese alloys since only longitudinal or nearly longitudinal ordering is observed (ordered magnetic moments are either parallel to Q_0 or the ordered magnetic moment component perpendicular to Q_0 is very small). Two different components of the static susceptibility tensor were observed above T_N by Ishikawa *et al* (1973). One can rewrite (2) in a more general form:

$$\chi_{Q\perp}^{-1}(Q, \omega) = \chi_{Q\perp}^{-1}(Q_0, 0) + a_1 q^2 - \mathrm{i}c_1\omega \tag{4a}$$

$$\chi_{Q\parallel}^{-1}(Q, \omega) = \chi_{Q\parallel}^{-1}(Q_0, 0) + a_2 q^2 - \mathrm{i}c_2\omega. \tag{4b}$$

Both components contribute to the scattering cross-section in a way defined by the two different staggered susceptibilities and the two different spectral widths:

$$\Gamma_\perp(q) = \Gamma_{0\perp} + A_1 q^2 \qquad \Gamma_{0\perp} = c_1^{-1}\chi_{Q\perp}^{-1}(Q_0, 0) \qquad A_1 = a_1 c_1^{-1} \tag{5a}$$

$$\Gamma_\parallel(q) = \Gamma_{0\parallel} + A_2 q^2 \qquad \Gamma_{0\parallel} = c_2^{-1}\chi_{Q\parallel}^{-1}(Q_0, 0) \qquad A_2 = a_2 c_2^{-1}. \tag{5b}$$

Below T_N we must distinguish the longitudinal and transverse components of the susceptibility tensor. We shall consider expansions around the true MBZ centre given by the Q_{01} vector and around the 'unfulfilled' MBZ centre described by the Q_{02} vector for the case of a single domain system.

Around Q_{01} which is the true MBZ centre the transverse component of the generalized susceptibility tensor is dominated by the spin waves and its imaginary part should have the form derived for the damped oscillator:

$$\mathrm{Im}\chi_\perp(Q, \omega) = \chi_\perp(Q_{01} + q, 0)\frac{\Gamma(q)\omega\omega_q}{(\omega^2 - \omega_q^2)^2 + \Gamma^2(q)\omega^2} \tag{6}$$

where ω_q is the frequency of the spin wave with the wavevector q, $\Gamma(q)$ is the damping ratio. $\chi_\perp(Q_{01} + q, 0)$ is the q-dependent static susceptibility usually given in the form: $\chi_\perp(Q_0 + q, 0) = \chi_\perp(Q_0, 0)\kappa^2/(\kappa^2 + q^2)$, where κ is the inverse correlation length.

The longitudinal component of the susceptibility around Q_{01} should be approximated below T_N by the expression similar to that above T_N:

$$\chi_\parallel^{-1}(Q, \omega) = \chi_\parallel^{-1}(Q_{01}, 0) + a_2 q^2 - \mathrm{i}c_2\omega. \tag{7}$$

The neutron scattering cross-section for the longitudinal component of the susceptibility below T_N has the same form as equation (3) as for scattering above T_N with $\Gamma(q)$ defined by a_2, c_2 and $\chi_\parallel(Q_{01}, 0)$.

The approximation around the 'unfulfilled' MBZ centre (for $Q \cong Q_{02}$) has been considered so far only for the incommensurate SDW structure in chromium (Sato and Maki 1974). The values of the coefficients depend strongly on the specific model used for chromium but the general form of extension is valid around any 'unfulfilled' MBZ centre if there are no low energy spin waves around this point. The three diagonal components of the susceptibility tensor can be different. Since Q_{01} is parallel to the z axis and Q_{02} parallel to the x axis the three components of the susceptibility have the form:

$$\chi_{ZZ}^{-1}(Q, \omega) = \chi_{ZZ}^{-1}(Q_{02}, 0) + a_1 q^2 - \mathrm{i}c_1\omega \tag{8a}$$

$$\chi_{YY}^{-1}(Q, \omega) = \chi_{YY}^{-1}(Q_{02}, 0) + a_1 q^2 - \mathrm{i}c_1\omega \tag{8b}$$

$$\chi_{XX}^{-1}(Q, \omega) = \chi_{XX}^{-1}(Q_{02}, 0) + a_2 q^2 - \mathrm{i}c_2\omega. \tag{8c}$$

The staggered susceptibilities $\chi_{Q\parallel}(Q_{01}, 0, T)$, and $\chi_{XX}(Q_{02}, 0, T)$ diverge at T_N since they both tend to $\chi_{Q\parallel}(Q_0, 0, T = T_N)$. They are expected (see e.g. Collins 1989) to

depend strongly on temperature. For the simplest models this dependence is linear with $1/|T - T_N|$. The coefficients a_2 and c_2 should have similar values below and above T_N. One can expect the decrease of the INS intensity coming from longitudinal fluctuations around true MBZ centres and from longitudinal and transverse fluctuations around 'unfulfilled' MBZ centres, when temperature is lowered below T_N. Both components of the staggered susceptibility tensor: $\chi_{ZZ}(Q_{02}, 0, T)$ and $\chi_{YY}(Q_{02}, 0, T)$ which are perpendicular to Q_{02} tend to $\chi_{Q\perp}(Q_0, 0, T = T_N)$ but they are not expected to diverge if there is no instability against the transverse structure. We expect that both components perpendicular to Q_{02} are similar, particularly close to T_N and we shall neglect the difference between them. We expect also that the coefficients A_1 of the q dependence of the spectral width $\Gamma_\perp(q)$ for fluctuations perpendicular to Q_0 above T_N do not differ very much from those for fluctuations perpendicular to Q_{02} around 'unfulfilled' MBZ centres below T_N. The same expectation concerns A_2 for fluctuations parallel to Q_{02}.

We expect the same critical neutron scattering and the same inelastic neutron scattering above T_N around all points described by any of the Q_{0i} vectors ($i = 1, 2, 3$). Below T_N one expects the scattering on damped spin waves, which because of the high value of spin wave velocity could be observed not far from true MBZ centres and some extension of the critical scattering around 'unfulfilled' MBZ centres. The last effect is the main object of the present experiment.

Our consideration is valid if there are no low energy spin waves around Q_{02}. However some softening of the spin waves could be expected at this point in the alloys with the composition close to the phase boundaries between single-Q AF1, double-Q AF1 and triple-Q AF1 (Long and Yeung 1986).

The low energy spin waves with quadratic dispersion relation were also predicted at the MBZ boundary point connected to the Q_{02} vector by Kouvel (1971). If the low energy spin waves described by Kouvel are present and if they are strongly damped as spin waves at $Q = Q_{01}$, the formula (8*a*) for $\chi_{ZZ}(Q_{02}+q, \omega)$ is still valid but both susceptibility components perpendicular to the magnetic moments $\chi_{XX}(Q_{02} + q, \omega)$ and $\chi_{YY}(Q_{02} + q, \omega)$ are dominated by the spin waves. We obtain then the formulae analogous to (6)

$$\mathrm{Im}\chi_{XX}(Q, \omega) = \chi_{XX}(Q_{02} + q, 0)\frac{\Gamma_2(q)\omega\omega_{2q}}{(\omega^2 - \omega_{2q}^2)^2 + \Gamma_2^2(q)\omega^2} \tag{9a}$$

$$\mathrm{Im}\chi_{YY}(Q, \omega) = \chi_{YY}(Q_{02} + q, 0)\frac{\Gamma_2(q)\omega\omega_{2q}}{(\omega^2 - \omega_{2q}^2)^2 + \Gamma_2^2(q)\omega^2}. \tag{9b}$$

The components of the static susceptibility $\chi_{XX}(Q_{02} + q, 0)$ and $\chi_{YY}(Q_{02} + q, 0)$ should be different since their behaviour close to T_N is different, as written above.

The spin wave dispersion relation around the MBZ centre and around boundary point defined by Q_{02} was obtained by Kouvel for low temperatures. The q dependence of the spin wave frequency close to Q_{02} is found to be quadratic and anisotropic. The energy gap for $Q = Q_{02}$ is always smaller than that for $Q = Q_{01}$, thus the low energy spin waves should be observed at both points at low temperature. For parameters realistic for γ-Mn alloys and for energy much higher than the energy gaps, the spin wave dispersion relations expanded around both points have a similar shape and should have a similar temperature dependence.

Damping of the spin waves was not obtained by Kouvel but one can expect damping which increases with temperature at least at temperatures close to T_N.

The modes observed by us at the MBZ boundary have completely different temperature behaviour, as will be shown in the next section and in section 4.3.

3. Experimental procedures

The present experiment was performed on the Mn(13.7% Ni) sample used earlier to study the spin waves around the magnetic Brillouin zone centre (Jankowska-Kisielińska *et al* 1997a, called hereafterafter I). The alloy is a single-Q AF1-type antiferromagnet below $T_N = 480$ K. In the antiferromagnetic phase there is a tetragonal distortion of the lattice, with $1-c/a = 0.027$ at room temperature. The crystal structure becomes bct with two simple tetragonal magnetic sublattices. However the bct terminology is not very convenient for comparing the results for different phases of γ-manganese alloys. The notation 'fct' is used for the tetragonal structure in the literature (e.g. Honda *et al* 1976). The pseudo-fcc notation for the reciprocal lattice is also used in the literature of similar systems (e.g. Hälg and Furrer 1986).

The magnetic moments are oriented mainly along the Q_{01} direction (longitudinal ordering) and give no Bragg reflection at (001). However we observe the low intensity reflections at (001), (010) and (100). They are similar to those observed in Mn–Cu alloys described by us some time ago (Jankowska *et al* 1982). Since their intensity (corrected for the form factor) is less than 0.8% of the intensity at (110), due to the longitudinal AF1 ordering, we neglect them when analysing inelastic neutron scattering, but they should be probably taken into account for small energy transfers.

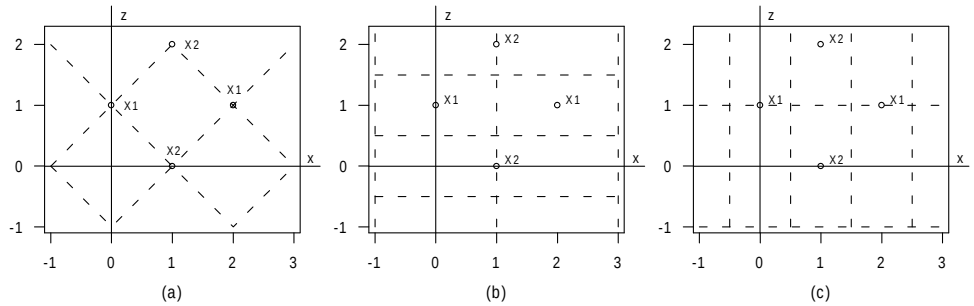

Figure 1. The reciprocal pseudo-fcc lattice points and MBZ boundaries in the scattering plane for three types of domain. Figure 1(a) is the scattering plane for 55% of domains, which have Q_{01} perpendicular to the scattering plane, figure 1(b) is for 37% of domains with Q_{01} along the [001] direction and figure 1(c) is for 8% of domains with Q_{01} along the [100] direction.

The population distribution of domains with the antiferromagnetic Q_{01} vector oriented along each of three main crystal axes was determined as described in I. At room temperature the populations of domains with Q_{01} oriented along [010], [001] and [100] were found to be: $55 \pm 11\%$, $37 \pm 5\%$ and $8 \pm 2\%$ respectively. This distribution is stabilized by the tetragonal lattice deformation. The accurate domain distribution measurements were not made at each temperature. Instead we have tested the domain distribution stability comparing the Bragg peak intensities connected to differently oriented domains. We conclude that, at least up to 450 K the domain distribution has not changed. We also observed that even after heating the sample to about 70 K above T_N, where fcc structure is obtained, and cooling it to the room temperature the domains have the same population distribution, within the experimental error.

The INS measurements were performed by means of a three-axis neutron spectrometer 1T, installed on a thermal beam at the Orphee reactor in the Laboratoire Léon Brillouin CEN, Saclay. We have measured and compared the temperature dependence of the inelastic scattering in two types of reciprocal lattice point: (1) the (001) and (201) rlps which are the MBZ (magnetic Brillouin zone) centres for 37% of domains (named X1 in figure 1) and (2) the (100)

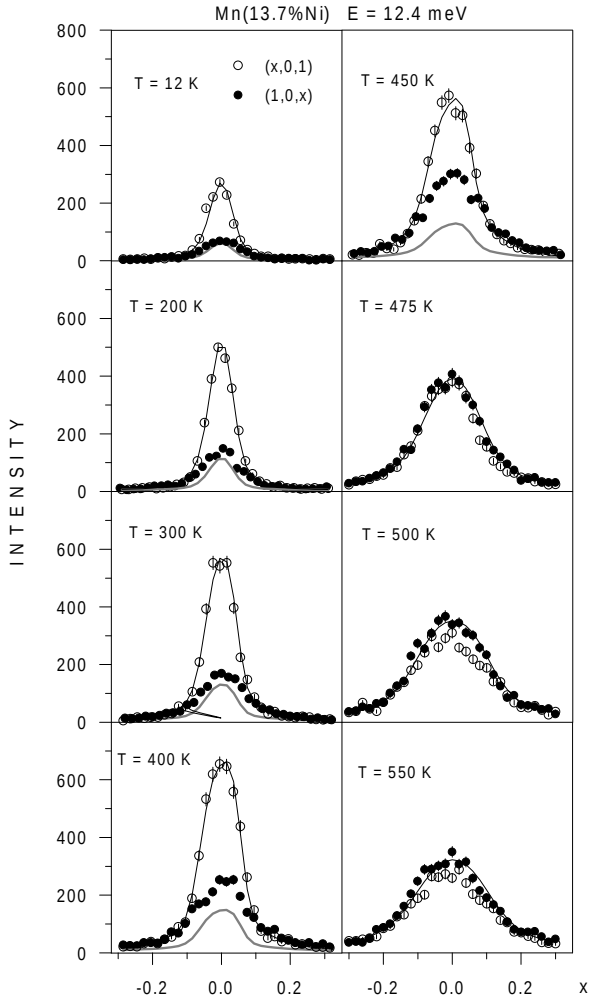

Figure 2. The intensity distributions versus momentum transfer for energy transfer 12.4 meV measured around the (001) and (100) rlps at different temperatures. The thin black line is the computed distribution around the (001) rlp and the thick grey line is the same distribution multiplied by the domain population ratio 0.22.

and (102) rlps which are the MBZ centres for 8% of domains (named X2 in figure 1). The reciprocal pseudo-fcc lattice points and MBZ boundaries in the scattering plane are presented in figure 1 for three types of domain. Figure 1(a) is the scattering plane for 55% of domains, which have Q_{01} perpendicular to the scattering plane, figure 1(b) is for 37% of domains with Q_{01} along the [001] direction and figure 1(c) is for 8% of domains with Q_{01} along the [100] direction. The [100] and [001] directions have their fct meaning for domains oriented as shown in figure 1(b). The measurements were performed with constant scattered neutron energy $E_f = 14.7$ meV. The horizontal collimations starting from the reactor core were 26′–30′–40′–60′. The intensity distributions versus momentum transfer for energy transfers 12.4 meV, 16.54 meV and 22.74 meV around the (001) and (100) rlps and for energy transfer 53.76 meV around the (201) and (102) rlps were measured in the temperature range 12–550 K.

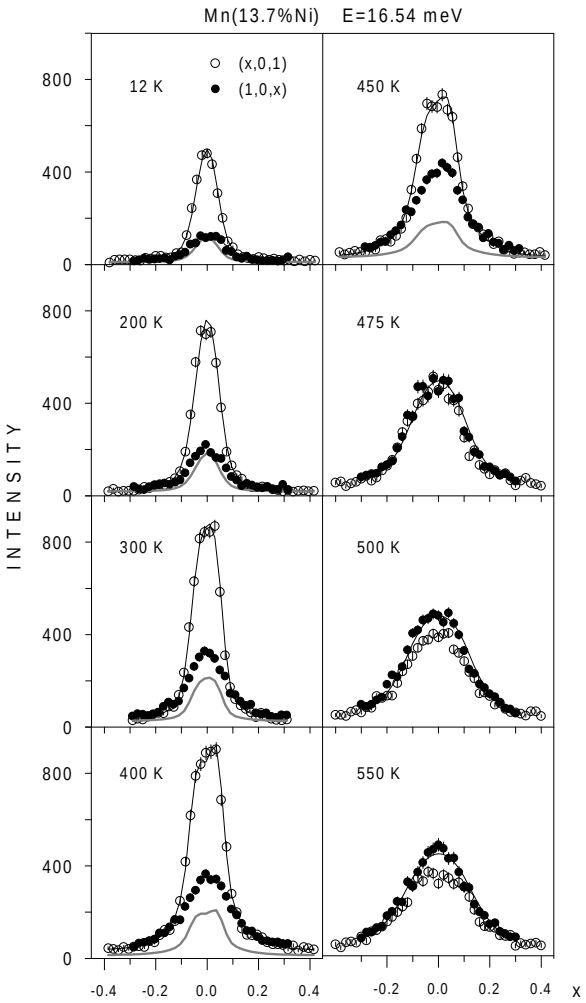

Figure 3. The intensity distributions versus momentum transfer for energy transfer 16.54 meV measured around (001) and (100) rlps at different temperatures. The marking is the same as in figure 2.

The unequal domain population allows us to estimate the intensity distributions around MBZ centres and around the points on the MBZ boundary equivalent crystallographically to the MBZ centre, which can be named 'unfulfilled' MBZ centres. The measurements above T_N were taken also around the points of different types although they are expected to give the same results.

Special attention was paid to estimating properly the intensity of the incoherent scattering. The additional energy distribution was measured up to 33 meV far from the Brillouin zone centre at 350 K. It was used to estimate the incoherent scattering at other temperatures corrected for the population factor.

The measured distributions around the (001) and (100) rlps for energy transfer 12.4 meV and 16.54 meV are presented in figures 2 and 3 for different temperatures. At the lowest temperature the ratio of the maximum intensity measured around the (100) rlp to that around

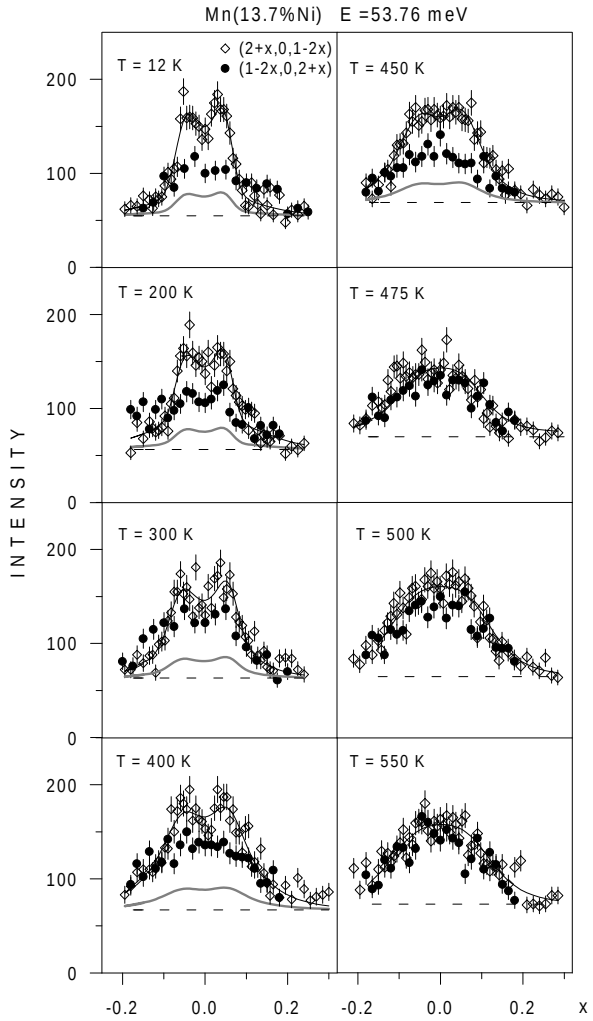

Figure 4. The intensity distributions versus momentum transfer for energy transfer 53.76 meV measured around (201) and (102) rlps at different temperatures. The thin black line is the computed distribution around the (201) rlp and the thick grey line is the same distribution multiplied by the domain population ratio 0.22. The black dashed line is the background plus the incoherent scattering level.

the (001) rlp is equal to 0.22 i.e. to the ratio of the populations of the domains with the Q_{01} vector oriented along [001] and [100] directions. In figures 2 and 3 the experimental points for 12 K obtained around the (100) point are placed well at the line fitted to the points measured around (001) scaled by the factor 0.22. The whole scattering can be ascribed to the spin waves with wavevectors close to the MBZ centre. There is no evidence for the spin waves predicted by Kouvel. The ratio of the maximum intensity at (100) to that at (001) increases from 0.22 at 12 K up to 1 at the Néel temperature. The scattering centred around the MBZ boundary point equivalent to the MBZ centre starts to be evident for 12.4 meV and 16.54 meV at 300 K, when the intensity measured around (100) is evidently higher than the scaled intensity around (001). At T_N and above it the intensity distributions around both points are roughly the same, as expected since in the paramagnetic phase the above mentioned two types of point are identical.

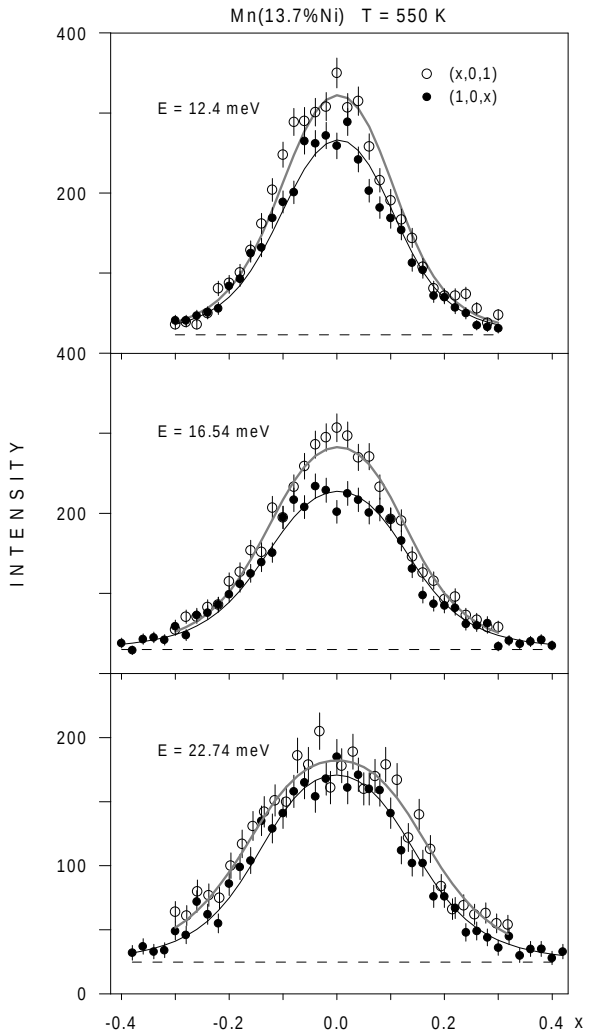

Figure 5. The intensity distributions versus momentum transfer for energy transfer 12.4 meV, 16.54 meV and 22.74 meV measured around (001) and (100) rlps at 550 K. The solid thin and thick lines are the calculated (as a convolution of the neutron scattering cross-section with the spectrometer resolution function) intensity distributions around the (001) and (100) rlps respectively.

Small differences of the intensity are probably due to small geometrical differences. Results for energy 22.74 meV are similar.

For energy transfer 53.76 meV the intensity distributions around (201) and (102) presented in figure 4 have evidently different shapes at temperatures from 12 K up to 400 K. Distributions around (201) demonstrate two separate maxima for '+' and '−' q. The distributions around (102) are more 'diffusive type'. Even at the lowest temperature the ratio of the maximum intensity of scattering around (102) to that around (201) is bigger than that resulting from the domain population distribution (0.22). The scattering around the 'unfulfilled' MBZ centre is present even at the lowest temperature. Its intensity increases slowly with temperature. At T_N and above it the distributions around both points are similar.

4. Data analysis

Most of our measurements were performed around the (001) or (100) rlp where only the component of the susceptibility tensor which is perpendicular to the Q_0 vector contributes to the cross-section. The reason is the term in the first brackets of equation (1) and the small value of $q = |Q - Q_0|$. The measurements around the (201) and (102) rlps can contain the contribution of the components perpendicular and parallel to the Q_0 vector ([001] and [100] respectively).

4.1. Inelastic neutron scattering above T_N

Data obtained above T_N were analysed in terms of Lorentzian type cross-section as given by formulae (3), (4) and (5). This is justified for scans around (100) and (001) points for energy transfers 12.4, 16.54 and 22.74 meV. When analysing the data for energy transfer 53.76 meV measured around the (201) and (102) points one should take into account both components of the susceptibility: one perpendicular and the other parallel to the Q_0 vector, but one would have too many parameters for the fitting procedure. We decided to treat the data obtained around (201) and (102) in the same way as data around (001) and (100) taking into account only one component, just for a test, since we can expect that the component perpendicular to the Q_0 vector dominates at temperatures not very close to T_N.

Examples of the measured and calculated (as the convolution of neutron scattering cross-section with the spectrometer resolution function) intensity distributions are shown in figure 5. The difference between results for the two types of point is that the intensity is slightly higher for the (100) point. This is probably due to the small geometrical difference.

The value of the parameter A derived by fitting to the data obtained at 500 K (222 ± 30 meV Å^2) is somewhat higher than for 550 K (200 ± 16 meV Å^2). The determination of the value of Γ_0 is not very accurate since the intensity measured around $q = 0$ and $\omega = 0$ has several components. We obtained $\Gamma_0 \sim 2$ meV at 500 K and $\Gamma_0 \sim 4.5$ meV at 550 K. We tried also to fit in the same way the data for the temperature 475 K, which is ~5 K below T_N. We obtained $A = 358 \pm 44$ meV Å^2 and $\Gamma_0 = 3.30 \pm 0.1$ meV, but probably at this temperature the used formulae are oversimplified.

It might be interesting to compare our results with those obtained by Yazaki *et al* (1994) for the typical Heisenberg antiferromagnet $RbMnF_3$ and for the intermetallic compound Mn_3Pt. For Mn_3Pt they obtained a comparable value of A: 360 meV Å^2 at 1.1 T_N and 340 meV Å^2 at 1.2 T_N for the [010] direction and a value for the [100] direction which is lower by one order of magnitude. For $RbMnF_3$ the value of A was 10 meV Å^2 at 1.2 T_N. We confirm their conclusion that in metals the value of A is at least one order of magnitude higher than in typical Heisenberg magnets.

4.2. Spin waves at low temperatures

Data obtained at 12 K for energy transfers 12.4, 16.54 and 22.74 meV were analysed in terms of the spin waves only. The results obtained for low temperatures are summarized in table 1.

In our previous experiment (I) we obtained at 100 K spin wave velocity $v = 231 \pm 16$ meV Å, energy gap $E_g = 8.9 \pm 0.5$ meV and damping parameter $\Gamma_1 = 113 \pm 58$ meV Å. The values of the velocity and energy gap in the spin wave dispersion relation obtained in our previous experiment are consistent with the present results. The values of damping parameter obtained in the present experiment are evidently higher than in the previous one. These values are more reliable as they were derived by a more accurate data analysis.

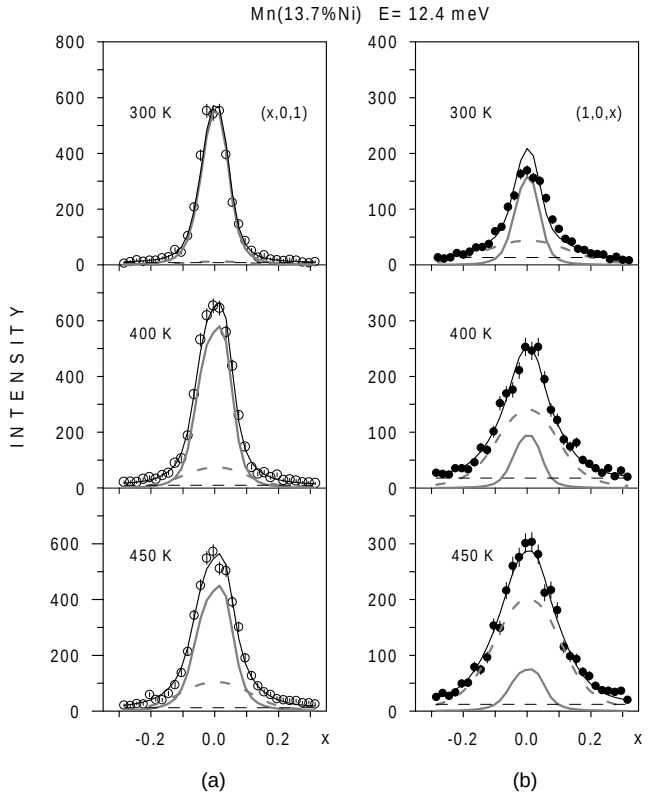

Figure 6. The estimated components of the observed distributions for energy transfer 12.4 meV measured around the (001) (a) and (100) (b) rlps at different temperatures. The black solid line is the computed distribution of the total intensity, the thick grey line is the spin wave component of the intensity, the thick dashed grey line is the component coming from the 'unfulfilled' MBZ centre and the thin dashed line is the background plus the incoherent scattering level.

Table 1. The parameters of the spin wave dispersion relation and damping in Mn(13.7% Ni) alloy for low temperatures.

T [K]	v [meV Å]	E_g [meV]	Γ_1 [meV Å]
12	250 ± 10	9.38 ± 0.23	178 ± 16
~ 100	—	9.54 ± 0.25	—
~ 200	234 ± 6	8.90 ± 0.19	220 ± 25

4.3. Intermediate temperatures below T_N

In the analysis of data obtained below T_N two components of neutron scattering intensity were taken into account: (1) the scattering around the true MBZ centre described by the scattering cross-section for damped spin waves (equation (6) and (2) the scattering around 'unfulfilled' MBZ centres described by the Lorentzian-type cross-section for diffusive excitations (equation (3)). These two components were taken in proportion deduced from the domain population distribution.

For energy transfer 12.4 meV the separated components of intensity distribution measured around (001) are presented in figure 6(a) and around the (100) point in figure 6(b). Figure 7(a), (b) is a similar presentation for the energy transfer 22.74 meV.

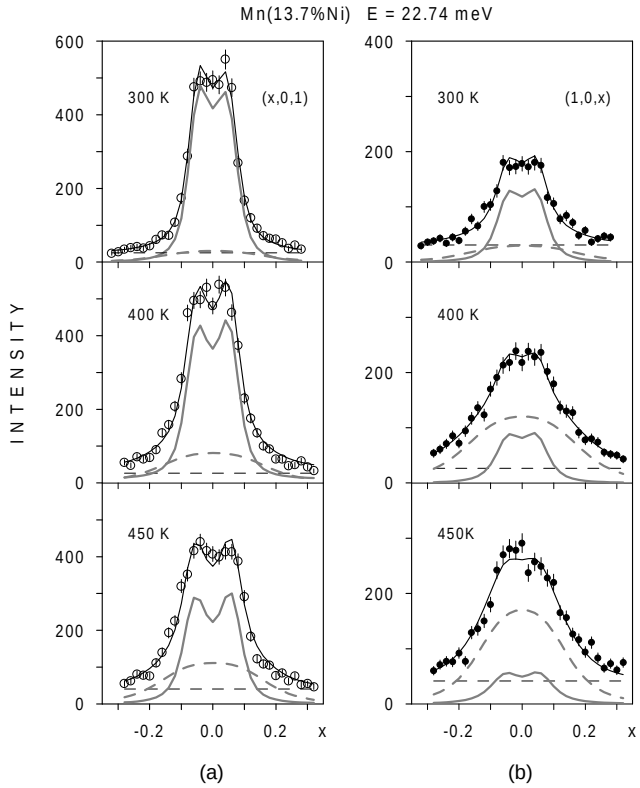

Figure 7. The estimated components of the observed distributions for energy transfer 22.74 meV measured around the (001) (a) and (100) (b) rlps at different temperatures. The marking is the same as in figure 6.

There is a significant difference in the temperature and energy dependence of both components. Such a difference is an additional argument against the description of the excitations around the 'unfulfilled' MBZ centre in terms of Kouvel modes. The intensity of the component connected to the 'unfulfilled' MBZ centre decreases when the temperature is lowered. This decrease is faster for lower energies. The intensity of the component originating from the spin waves increases slightly when the temperature is lowered from T_N to 300 K. Below T_N the intensity of the component connected to the 'unfulfilled' MBZ centre depends on energy more weakly than the intensity connected with the spin waves.

An attempt to separate the components of the observed intensity distributions for energy transfer 53.76 meV around (201) and (102) points is presented in figure 8(a), (b)). The temperature dependence of the intensity of both components seems to be more complicated since the intensity of the distribution measured around the 'unfulfilled' MBZ centre at 450 K is lower than that for 400 K and for 475 K. This result may be accidental.

The distributions presented in figures 6(a), 7(a) and 8(a) were measured around the reciprocal lattice points which are the MBZ centres for 37% of domains. The situation is very similar to that for the polydomain sample with equal domain distribution, where it is impossible to identify the components of the intensity. From the above mentioned figures it is clear that the spin wave measurements around the MBZ centre in polydomain samples are affected by the contributions coming from the surroundings of the MBZ boundary. This effect is more pronounced close to T_N and/or at higher energy.

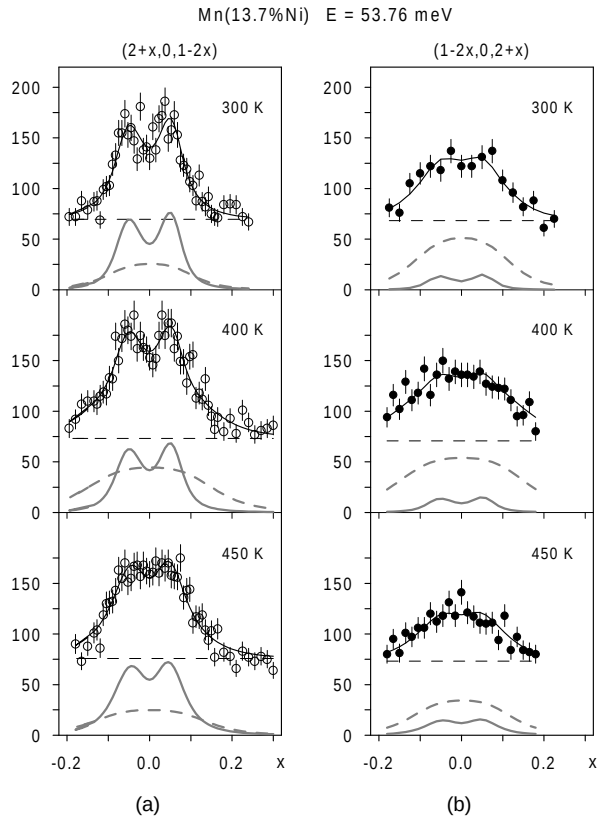

Figure 8. The estimated components of the observed distributions for energy transfer 53.76 meV measured around the (201) (a) and (102) (b) rlps at different temperatures. The marking is the same as in figure 6.

Parameters of the spin wave dispersion relation and damping obtained for the intermediate temperatures are presented in table 2.

Table 2. The parameters of the spin wave dispersion relation and damping in Mn(13.7% Ni) alloy for intermediate temperatures.

T [K]	v [meV Å]	E_g [meV]	Γ_1 [meV Å]
∼300	207 ± 11	6.7 ± 0.2	153 ± 33
∼400	188 ± 16	3.8 ± 1.0	169 ± 23
450	177 ± 12	4.0 ± 0.2	154 ± 23

The spin wave velocity obtained in the present experiment has higher values than in the previous experiment and it is less temperature dependent. The damping parameter obtained now has the values higher than the previous ones but in both cases it does not depend on temperature within the accuracy of its determination. The values of damping parameter obtained in the present experiment are more reliable since we have paid more attention to proper estimation of the background and the incoherent scattering. The accuracy of the determination of the damping parameter depends very strongly on the accuracy of estimate of these factors.

The scattering around the 'unfulfilled' MBZ centre was treated in terms of the Lorentzian-type cross-section with spectral width $\Gamma(q)$ in the hydrodynamic form:

$$\Gamma(q) = \Gamma_0 + Aq^2.$$

The parameters of the spectral width Γ_0 and A should be obtained by a fitting procedure from $I(E)$ and $I(q)$ distributions around the (100) point, while for the spin wave component the parameters are estimated on the basis of the distributions around the (001) point. The parameter Γ_0 should be obtained from the energy dependent distributions. Unfortunately these distributions are very complex for small energies probably because of the presence of a small transverse component of the magnetic moment mentioned in section 3 and it was impossible to separate all components in order to derive the values of Γ_0 accurately. The obtained values vary between 3.5 ± 0.3 meV and 4.9 ± 0.6 meV. We assumed some 'reasonable' values of Γ_0 in this range and tried to derive the values of parameter A from $I(q)$ distributions. The results are presented in table 3.

Table 3. The parameter A of the spectral width obtained for assumed Γ_0 from distributions around the 'unfulfilled' MBZ centre for intermediate temperatures. The values of κ are calculated according to $\kappa = \sqrt{A/\Gamma_0}$.

T [K]	Γ_0 [meV]	A [meV Å^2]	κ [Å]
300	5	145 ± 18	0.19 ± 0.01
400	4	209 ± 34	0.14 ± 0.01
450	4	236 ± 31	0.13 ± 0.01

The obtained values of A are of the same order of magnitude as those obtained in the paramagnetic state. The temperature dependence of the parameter A is consistent with expectations described in section 2. The very weak temperature dependence of parameter Γ_0 is probably caused by the anisotropy yielding the difference between the longitudinal and transverse components of the susceptibility.

The reciprocal correlation length κ was not measured independently but we derived it from the parameters Γ_0 and A. The temperature dependence of κ is weak and indicates nonzero value of κ at T_N. The finite value of κ at T_N for transverse fluctuations was observed in other manganese alloys with continuous phase transition, Mn(37% Fe) and Mn(38% Ni) (Milczarek *et al* 1989). This feature of the transverse fluctuations is caused by the anisotropy interactions yielding the longitudinal ordering below T_N.

5. Summary and conclusions

This is the first systematic study of the spin excitations around the MBZ boundary points equivalent to the MBZ centre in γ-Mn alloy. The magnetic inelastic neutron scattering was measured in the antiferromagnetic Mn(13.7% Ni) alloy in the sample with unequal domain distribution in the temperature range $0.025\,T_N$–$1.15\,T_N$. Measurements were performed around two types of reciprocal lattice point: one, which is the magnetic Brillouin zone centre for 37% of domains and the other which is the MBZ centres for 8% of domains. This allows us to separate the intensity of INS coming from the scattering around MBZ centres and that coming from the points on MBZ boundary equivalent crystallographically to the MBZ centres, which we named 'unfulfilled' MBZ centres.

The main result of our experiment is the evidence of the inelastic neutron scattering around the 'unfulfilled' MBZ centres in the temperature range from 300 K up to T_N for medium energies (12.4–22.7 meV) and from lowest temperature up to T_N for higher energy

(53.76 meV). The intensity of this scattering increases with temperature. The profiles of the $I(q)$ distributions around the 'unfulfilled' MBZ centres are broader than those around the MBZ centres at room temperature and they become identical at the temperature 475 K, very close to T_N. This temperature dependence suggests the explanation of the observed INS in terms of the extension of the critical scattering, rather than in terms of the low energy spin waves at the MBZ boundary as e.g. predicted by Kouvel (1971) or soft spin waves (Long and Yeung 1986).

The analysis performed in terms of the extension of the critical scattering is fairly consistent. The obtained temperature dependence of the parameters of the spectral width agrees qualitatively with the general features of spin fluctuations.

The present results provide the explanation of our doubts regarding the nature of the INS at the 'unfulfilled' MBZ centre observed for the first time in Mn(18% Cu) alloy (Mikke *et al* 1983).

In our work on an Mn(12% Ge) polydomain sample (Jankowska-Kisielińska *et al* 1997b) we suggested that the observed inelastic neutron scattering in the temperature range from 150–200 K below T_N up to T_N is difficult to understand in terms of damped spin waves solely and that another type of excitation contributes to the observed intensity. This suggestion is supported by the present results and the character of these additional excitations is identified.

In the paramagnetic temperature range the overall behaviour of the INS in 3d antiferromagnets and ferromagnets is similar. This refers in particular to the weak temperature dependence of the intensity and localization of the INS profiles in q space.

We described the INS observed above T_N in terms of hydrodynamic formulae for paramagnetic scattering. The obtained values of the spectral width parameters for the paramagnetic region are rather close to those describing the INS around the 'unfulfilled' MBZ centres in the antiferromagnetic region. The obtained value of the magnetic stiffness parameter at similar T/T_N is of the same order of magnitude as that for the intermetallic compound Mn_3Pt and is by one order of magnitude higher than for the typical Heisenberg antiferromagnet $RbMnF_3$.

Acknowledgments

This work was partly supported by the 'Human Capital and Mobility—Access to Large Scale Facilities' PECO Extension Programme (contract No ERB CIPD CT 940080) and partly by the State Committee for Scientific Research, Poland (under KBN contract No 2 P03B 071 13).

References

Böni P, Mook H A, Martinez J L and Shirane G 1993 *Phys. Rev.* B **47** 3171–9
Collins M F 1989 *Magnetic Critical Scattering* (Oxford: Oxford University Press)
Halperin B I and Hohenberg P C 1969 *Phys. Rev.* **177** 952–71
Hälg, B and Furrer A 1986 *Phys. Rev.* B **34** 6258–79
Honda N, Tanji Y and Nakagawa Y 1976 *J. Phys. Soc. Japan* **41** 1931–7
Ishikawa Y, Endoh Y and Ikeda S 1973 *J. Phys. Soc. Japan* **35** 1616–26
Izuyama T, Kim D J and Kubo R 1963 *J. Phys. Soc. Japan* **18** 1025–42
Jankowska J, Mikke K, Vintaikin E Z and Udovenko V A 1982 *J. Magn. Magn. Mater.* **27** 41–8
Jankowska-Kisielińska J, Mikke K and Milczarek J J 1997a *J. Phys.: Condens. Matter* **9** 10 761–76
Jankowska-Kisielińska J, Mikke K, Milczarek J J, Hennion B and Udovenko V A 1997b *Acta Phys. Pol.* A **91** 483–6
Kouvel J S 1971 *J. Physique Coll.* **32** C1 695–6
Long M W and Yeung W 1986 *J. Phys. F: Met. Phys.* **16** 769–90
Milczarek J J, Jaworska E and Mikke K 1989 *Physica* B **156/157** 238–40
Mikke K, Jankowska J and Jaworska E 1983 *J. Magn. Magn. Mater.* **31–34** 125–6
Mikke K, Jankowska-Kisielińska J and Hennion B 1998 *Physica* B **241–243** 609–12

Moriya T 1985 *Spin Fluctuations in Itinerant Electron Magnetism* (Berlin: Springer)
Sato H and Maki K 1974 *Int. J. Magn.* **6** 183–209
Sternlieb B J, Hill J P, Inami T, Shirane G, Lee W T, Werner S A and Fawcett E 1995 *Phys. Rev. Lett.* **25** 541–4
Van Hove L 1954 *Phys. Rev.* **95** 1374–84
Vintaykin E Z, Udovenko V A, Mikke K and Jankowska J 1981 *Solid State Comm.* **37** 295–7
Yazaki A, Tajima K, Todate Y, Tomiyoshi S and Ikeda H 1994 *J. Phys. Soc. Japan* **63** 748–54